

**Supporting Information for “Nanometer Distance Measurements Between  
Multicolor Quantum Dots”**

**J. Antelman, C. Wilking-Chang, S. Weiss, X. Michalet**

**1. Supporting Material and Methods**

**Preparation of QD-dimers**

*Method 1:* 60 or 90 bp biotinylated oligonucleotides (C6-linker) were purchased from Integrated DNA Technologies (Coralville, IA).

Sequence for 60 bp: 5' - /5Biotin/TCC AGG TCA CCA GTG CAG TGC TTG ATA  
ACA GGA GTC TTC CCA GGA TGG CGA ACA ACA AGA – 3'

Complementary sequence for 60 bp: 5' - /5Biotin/TCT TGT TGT TCG CCA TCC  
TGG GAA GAC TCC TGT TAT CAA GCA CTG CAC TGG TGA CCT GGA – 3'

Sequence for 90 bp: 5' - /5Biotin/TCC AGG TCA CCA GTG CAG TGC TTG ATA  
ACA GGA GTC TTC CCA GGA TGG CGA ACA ACA AGA AAC TGG TTT CCG  
TCT TCA CGG ACT TCG TTG – 3'

Complementary sequence for 90 bp: 5' - /5Biotin/CAA CGA AGT CCG TGA AGA  
CGG AAA CCA GTT TCT TGT TGT TCG CCA TCC TGG GAA GAC TCC TGT TAT  
CAA GCA CTG CAC TGG TGA CCT GGA – 3'

For each type of dimer, one biotinylated sequence was mixed with 585 nm streptavidin-coated QDs (SAV-QD585) (Invitrogen, Carlsbad, California), while the complementary biotinylated sequence was separately mixed with SAV-QD655 as follows. 0.4  $\mu\text{l}$  of 1  $\mu\text{M}$  biotinylated 90 bp oligonucleotide was added to 7.6  $\mu\text{l}$  of 10 mM TE buffer (pH 7.8). This 8.0  $\mu\text{l}$  solution was added in 2  $\mu\text{l}$  aliquots (2  $\mu\text{l}$  every 5 min) to a 2  $\mu\text{l}$  solution of SAV-QD585 (stock solution, 1  $\mu\text{M}$ ), resulting in a final SAV-QD585: oligonucleotide molar ratio of 5: 1. The sample was incubated at room temperature (RT  $\sim$  25  $^{\circ}\text{C}$ ) for 30 min. Electrophoresis of this sample on a 1.5-2% agarose gel resulted in the separation of single DNA-QD products from free QDs, free DNA and products comprising multiple DNAs and QDs (Fig. 1A). The single DNA-QD band was extracted with a razor and the sample eluted using a “Freeze ‘N Squeeze DNA Gel Extraction” kit (BioRad, Hercules, CA) following the manufacturer’s protocol. 10  $\mu\text{l}$  of the SAV-QD585-oligonucleotide was then mixed with a 10  $\mu\text{l}$  solution of SAV-QD655-oligonucleotide containing the complementary sequence prepared similarly. The mixture was incubated at 55-65  $^{\circ}\text{C}$  for 5-10 min to hybridize the DNA strands, thus forming QD-dimers.

*Method 2:* 5  $\mu\text{l}$  of each of the two complementary 5' biotinylated oligonucleotides were mixed, resulting in a 10  $\mu\text{l}$  solution containing 50  $\mu\text{M}$  of each oligonucleotide in 10 mM TE buffer (pH 7.8). To promote hybridization of the complementary DNA strands, the oligonucleotides were heated in boiling water for 5 min and allowed to cool to RT over several hours. This dsDNA solution was diluted to 0.5  $\mu\text{M}$  and 6  $\mu\text{l}$  of this solution was added in aliquots (1  $\mu\text{l}$  every 10 min) to a 4  $\mu\text{l}$  solution containing 50 % of 1  $\mu\text{M}$  SAV-QD585 and 50 % of 1  $\mu\text{M}$  SAV-QD655. In this way, a mixture of SAV-

QD655/SAV-QD655 (25 %), SAV-QD585/SAV-QD585 (25 %) and SAV-QD585/SAV-QD655 (50 %) dimers was formed. However, the desired product (SAV-QD585/SAV-QD655) could be easily isolated during imaging to perform distance measurements as it was the only one to emit in both channels.

The first method produces more SAV-QD585/SAV-QD655 dimers but some deterioration of the QD's photo-stability was observed after a few days. Although we did not investigate this issue any further, it is possible that electrophoresis or the extraction protocol affects QD's photo-stability. In contrast, the second method did not seem to affect QD's fluorescence for at least several days. Note that, in both cases, we observed a significant variability from SAV-QD batch to SAV-QD batch as far as the width of the observed DNA-QD bands is concerned. In particular, in method 1, some batches did not allow a clear separation between single-DNA/single-QD complexes and QD-only, resulting in either smears or multiple bands, for reason that we have not been able to elucidate.

### **Blinking Suppression by DTT/Polymer Coating**

#1 Glass coverslips were thoroughly rinsed with acetone, methanol and milliQ water before use. QD-dimer solutions were diluted to single-molecule concentration before spin-coating of 10  $\mu$ l for 30 s at 3,500 rpm onto a clean glass coverslip. 20  $\mu$ l of a DTT-PVA polymer mixture (150 mM DTT, 1% PVA in milliQ H<sub>2</sub>O) was spin-coated for 30 s at 7,000 rpm on top of the QD or QD-dimer samples. This procedure almost totally eliminated QD's blinking, allowing long-term, high-resolution stage-scanning confocal imaging of QD-dimers (Fig. S1 & S2).

## **QD-Dimer Imaging**

The closed-loop stage-scanning confocal microscope used in these experiments was similar to that describe in ref. <sup>1, 2</sup>. The 488 nm line of an Ar ion laser (ILT 5490A, Midwest Laser Products, IL) was coupled to a single-mode fiber and collimated into the back of an oil immersion objective lens (NA 1.45) after expansion by a 10 x objective lens. Laser excitation was transmitted to the sample through a dichroic mirror (500 DCXT, Chroma Technology, Rockingham, VT). Fluorescence emission passed through the same dichroic mirror and was split in two components by a second dichroic mirror (630 LP, Chroma Technology) before filtering by bandpass filters (orange: 580 DF 70, Chroma Technology; red: 655 DF 25, Chroma Technology). A nm-resolution piezo-stage (Nano-LP200, MadCityLabs, Madison, WI) was controlled using two analog boards (PXI-6052E, PXI 6711, National Instruments, Austin, TX) and custom software written in LabView 7.1 (National Instruments or NI). The signals from the SPAD (SPCM-AQR 14, Perkin Elmer, Fremont, CA) were recordered using a counting board (PXI-6602, NI) controlled by the software.

To identify QD-dimers, 20 x 20  $\mu\text{m}$  low-resolution scans were first obtained (excitation power: 300-1000 nW, pixel integration time: 15 ms, pixel size: 250 nm). QD-dimer candidates were defined as co-localized spots in the 585 nm (yellow) and 655 nm (red) detection channels. Potential QD-dimer sites were then re-scanned with high-resolution (scan size: 1x1  $\mu\text{m}$ , excitation power: 500-1,000 nW, integration time: 10-15 ms, pixel size: 12.5 nm). Next, an emission time trace for each SPAD (655 and 585 nm) was recorded for  $\sim$ 1-2 min. The presence of only two intensity levels (on and off periods)

from each APD signal was taken as evidence that only 2 single QD's were present (655 and 585 nm) and that we were not imaging QD aggregates. When more than one QD was present at a particular emission wavelength, the emission time trace would indeed occasionally show multiple emission levels.

Note that although the images presented here were acquired with very high resolution (12.5 nm per pixel), identical distance resolution was obtained with much coarser image resolution (50 nm per pixel) and comparatively longer integration time per pixel, in agreement with theoretical expectation (data not shown)<sup>1,3</sup>.

### **QD localization and localization uncertainty**

In the case of a validated single QD in each channel, the acquired high-resolution images were used to precisely locate the center of each QD image (point-spread-function or PSF) as follows. Each image was fitted by least-square minimization to a tilted two-dimensional Gaussian after rejection of pixels with intensity below a threshold value equal to the standard deviation of the image intensity distribution. This allowed rejecting dark or poorly emitting pixels within the PSF. In general, a better adjustment of the threshold may allow keeping more pixels for the fit, but in our experience, this refinement did not significantly affect the fitting resolution. Each pixel was weighted by its value to the power  $-1/2$  as is appropriate for a shot-noise limited SPAD signal.

To estimate the uncertainty on QD localization obtained in this manner, we used a bootstrap error estimation approach<sup>1,4</sup>. Briefly, 1,000 replicas of the image pixel data set were formed as follows. Each image being comprised of  $i=1 \dots N$  pixels with value  $I_i$ , for each replica we randomly picked  $N$  pixels within the original image (thus potentially

omitting some pixels of the original image, and picking some more than once). The resulting data set (replica) was fitted using the same model as before, resulting in a new, slightly different center location. The reason for the difference in center location is that in each replica, some original pixels have been discarded (thus the algorithm does not have any constraint at those pixel locations), whereas some random pixels have been selected more than once (thus effectively increasing the statistical weight of these pixels in the least square minimization algorithm). The distribution of fitted replica locations was histogrammed and itself fitted to a tilted 2D Gaussian distribution, characterized by a center position  $(X_m, Y_m)$ , a minor and major axis standard deviations  $(\sigma_a, \sigma_b)$  and an angle specifying the orientation of the major axis with respect to the horizontal,  $\alpha$ .

In the captions of Fig. S1 and S2, we report the average bootstrap uncertainty as well as the uncertainty calculated with Eq. (17) of ref. <sup>3</sup> for comparison (which assumes that all pixels are “on” and that their intensity is only affected by shot-noise or detector noise), to emphasize the overly optimistic accuracy predicted by the standard shot-noise analysis.

### **Uncertainty on distance measurement**

Each QD of a dimer was located as described with a probability distribution fitted to a tilted 2D Gaussian. It is possible to numerically compute the resulting distance probability density function (PDF) by 2D integration (X. Michalet, in preparation). In general, for small localization uncertainties compared to the measured distance, as is the case in this experiment, the distance PDF is very close to a Gaussian distribution, characterized by a center value  $d_m$  and a standard deviation  $\sigma_D$ . These are the values reported in Fig. 2.

## **TEM Imaging**

Pelco copper grids of 400 mesh size and 3.0 mm OD (Ted Pella, Redding, CA) were coated with a thin film of parlodion and carbon. The grids were glow-discharged using high-voltage, alternating current, immediately before sample deposition. A small aliquot (5  $\mu$ L) of the sample was placed directly onto the grid for 1 min, then wicked with Whatman 4 filter paper, and immediately stained with a 1% solution of uranyl acetate in water for 1 min. The samples were air-dried and viewed under a Hitachi H-7000 electron microscope at an accelerating voltage of 75 kV. Negatives were developed and digitized using a Minolta Dimage Scan MultiPro scanner, resulting in a 0.6784 nm/pixel scale. Image analysis was performed visually on the raw images with ImageJ software by measuring the minimum and maximum distance between opposite sides of QD images. We estimated that the determination of the boundary between the background and lighter stained organic coating of the QD was performed with a  $\sim$  1 pixel uncertainty.

## **SPAD Alignment**

We briefly describe the subtle effect observed when performing high-resolution distance measurements with our scanning-stage confocal microscope. One of the first steps before imaging is alignment of the SPADs used to collect the fluorescence signal emitted in each QD wavelength range. This is performed using 3-axes micrometer translation-stages on which the SPADs are individually mounted (Fig. S3). The goal is to focus all the incoming light onto the small ( $\sim$  200  $\mu$ m diameter) sensitive area of the SPAD. Several methods can be used to achieve this goal such as (i) imaging a uniformly fluorescent solution, (ii) imaging small fluorescent nanobeads or (iii) imaging small

scatterers such as gold nanoparticles. In practice, this is done by monitoring the collected signal (by unit time, e.g. 10 ms) as one moves the SPAD along any of the 3 axes. By iterative optimization, it is possible to position the SPAD such that it will collect the largest possible signal. This should correspond to the SPAD aligned on the optical axis and in the focal plane of the collecting lens. A test of this alignment consists in exciting the fluorescence of small beads (100 nm diameter) with a single laser line and image isolated beads by stage-scanning confocal microscopy. In principle, the location of the center of the bead image detected by both SPADs should be identical. However, in practice we observed that for each new SPAD alignment, the bead image centers were offset by a constant amount (center-to-center distance) and characterized by a fixed orientation. This was checked for different alignments by repeatedly imaging a bead, fitting its position in each channel, and reporting the center-to-center distance and orientation. In general, this offset is smaller than 10 nm when the above protocol is followed and can easily be reduced to 1 nm when special care is taken during SPAD alignment. We also noticed that this offset can depend on the microscope focus.

This ensemble of observations leads us to the conclusion that this effect is due to slight differences in the PSF images formed on each SPAD's sensitive area, which remain to be more precisely characterized.

### **Effect of SPAD offset on the measured dimer distances**

Once characterized, the presence of a constant offset can easily be incorporated in the data analysis. For instance, a set of dimer distances measured with a fixed SPAD offset will be affected by a random vector contribution equal to the offset. For small SPAD

offsets, this random addition will only broaden the measured distance distribution, as shown on Fig. S4A, which shows the effect on a Gaussian distance distribution of  $40.4 \pm 3.4$  nm. For larger SPAD offsets ( $> 5$  nm), the distribution will progressively be split into two major peaks connected by a shallow bridge (Fig. S4A). As we do not observe such a distribution, we can be sure that we are not dealing with large SPAD offsets.

Fitting the distributions shown in Fig. S4A with Gaussians (which becomes unsatisfactory above  $\sim 5$  nm, but still gives an idea of the magnitude of the broadening, we observe that the distance distribution standard deviation  $\sigma$  increases quadratically with the SPAD offset (Fig. S4B). Similarly, the mean value of the distribution (or peak of the fitted Gaussian) is slightly offset with respect to the true mean value of the distance distribution (40.4 nm, see Fig. S4C).

As discussed in the text, we realized the SPAD offset issue after most of our data had already been acquired, leaving us with an uncertainty as far as which SPAD offset value to assume. Experimentally, we observed that by aligning the SPADs as usual, we routinely obtained SPAD offset values between 1 and 10 nm. Assuming a random distribution of SPAD offset values between 0 nm and a maximum SPAD offset  $X$  nm, we computed the effect on the measured distance distribution, as shown in Fig. S5A. Starting from a Gaussian distribution of  $40.4 \pm 1.4$  nm (the standard deviation corresponding to the QD shape dispersion effect), we observed that the distribution was broadened symmetrically, with a linear increase of the standard deviation as a function of the maximum offset  $X$  (Fig. S5B). The value of the mean distance (center of the distribution, Fig. S5C) was almost unaffected by SPAD offsets smaller than 10 nm.

To verify that the SPAD offset and intrinsic distance distribution standard deviation combined linearly, we then studied the effect of a fixed range of SPAD offset [0, 8 nm] on the width of the distance distribution (Fig. S6). Starting from a unique distance ( $\sigma = 0$  nm) and increasing it up to 5 nm (Fig. S6A), we verified that the resulting standard deviation increased linearly with the intrinsic standard deviation (Fig. S6B). For instance, starting from an intrinsic standard deviation of 1.4 nm due to QD-shape dispersion, a [0, 8 nm] random SPAD offset resulted in a quasi-Gaussian distance distribution with standard deviation 3.4 nm, as observed experimentally.

Note that although offsets smaller than 1 nm between two SPADs can be obtained, this might not be easily achievable when more than two SPADs are used (for 3 or more color colocalization studies).

## 2. Supplementary Figure Captions

Fig. S1: Characteristic images (A, B) and time traces (C, D) of blinking QDs. A, C: SAV-QD585, B, D: SAV-QD655. Each QD was excited with  $0.5 - 1 \mu\text{W}$  at 488 nm.  $80 \times 80$  pixel images were scanned with 18.75 nm steps and 15 ms integration time. Scale bar: 500 nm. Time traces were obtained by parking the QD's center on the optical axis and recording the emitted fluorescence intensity for  $\sim 2$  min. For each image, we indicate the average localization uncertainty obtained by bootstrap analysis ( $\langle\delta x\rangle_B$ ) as well as that obtained by standard shot-noise analysis ( $\langle\delta x\rangle_{\text{SN}}$ ) in nm.

Fig. S2. Characteristic images and time traces of non-blinking QDs obtained with DTT/PVA coating. A, C: SAV-QD585, B, D: SAV-QD655. Images and time traces were acquired as described in Fig. S1.

Fig. S3. Schematic description of the setup used in these experiments. A dichroic mirror DM splits the incoming fluorescence signal between two SPADs. The signal is filtered by a bandpass filter specific to the observed QD, and focused with a lens onto the sensitive area of the SPAD.

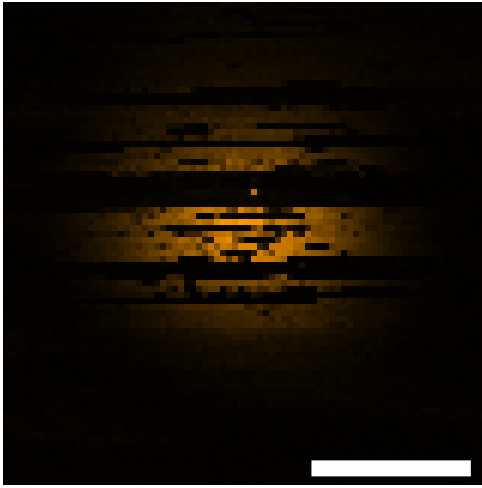
Fig. S4: Effect of fixed SPAD offset on measured distances. A: Histogram of  $10^5$  simulations of distances obtained from a true distance taken from a Gaussian distribution ( $d_m = 40.4$  nm,  $\sigma = 3.4$  nm) affected by a randomly oriented offset (indicated in nm in the Figure legend). B: Fitted standard deviation  $\sigma$  of the previous histograms. The evolution of  $\sigma$  is a quadratic function of the offset, indicating a broadening of the distance distribution. C: Shift of the measured distance as a function of SPAD offset. The shift is smaller than 1 nm for offsets up to 10 nm.

Fig. S5: Effect of variable SPAD offset on measured distances. A: Histogram of  $10^5$  simulations of distances obtained from a true distance taken from a Gaussian distribution ( $d_m = 40.4$  nm,  $\sigma = 1.4$  nm) affected by a randomly oriented variable offset (the maximum offset value is indicated in nm in the Figure legend). B: Fitted standard deviation  $\sigma$  of the previous histograms. The evolution of  $\sigma$  is a linear function of the offset, indicating a broadening of the distance distribution. C: Shift of the measured distance as a function of SPAD offset. The shift is smaller than 0.2 nm for offsets up to 10 nm.

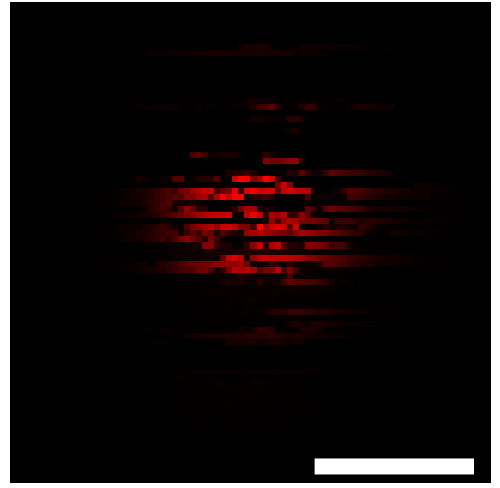
Fig. S6: Dependence of the histogram broadening as a function of initial distance distribution standard deviation. A: Simulation data for variable initial standard deviation of the distance (value in nm indicated in the legend), and a fixed range [0, 8 nm] of random offset values. B: Fitted standard deviation of the previous histograms, indicating a linear broadening. The dashed lines indicate the initial distance standard deviation due to the QD size variation (1.4 nm) and the broadening resulting from a random SPAD offset in the range [0, 8 nm] (final  $\sigma = 3.4$  nm).

### 3. Supplementary References

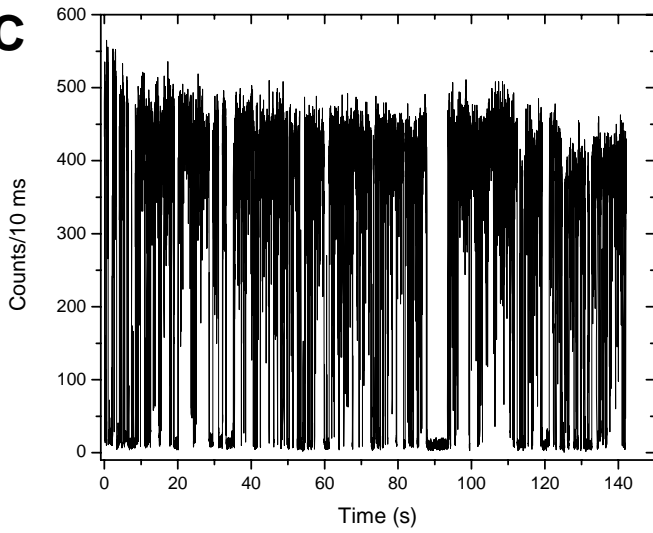
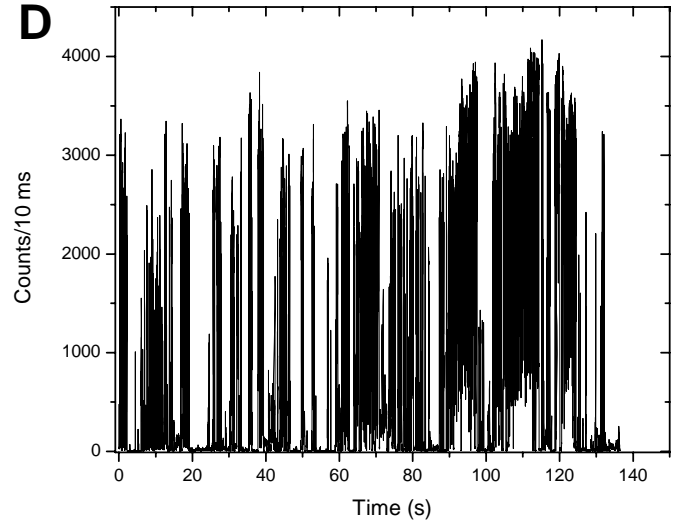
1. Michalet, X.; Lacoste, T. D.; Weiss, S. *Methods* **2001**, 25, (1), 87-102.
2. Lacoste, T. D.; Michalet, X.; Pinaud, F.; Chemla, D. S.; Alivisatos, A. P.; Weiss, S. *Proceedings of the National Academy of Sciences USA* **2000**, 97, (17), 9461–9466.
3. Thompson, R. E.; Larson, D. R.; Webb, W. W. *Biophys. J.* **2002**, 82, 2775-2783.
4. Efros, A. L.; Rosen, M. *Physical Review Letters* **1997**, 78, (6), 1110-13.

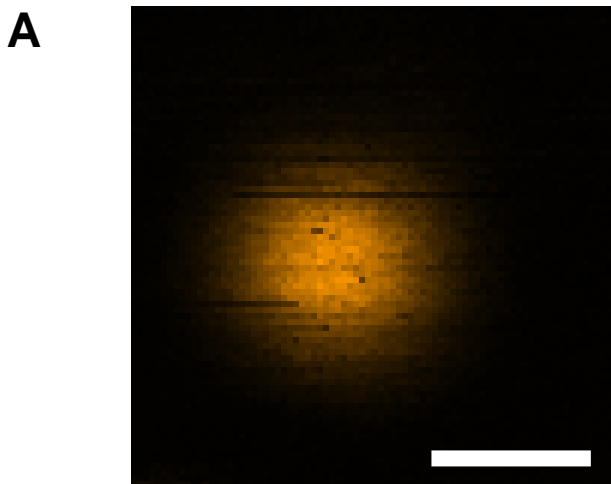
**A**

$$\langle \delta x \rangle_B = 1.9 \text{ nm}$$
$$\langle \delta x \rangle_{SN} = 0.4 \text{ nm}$$

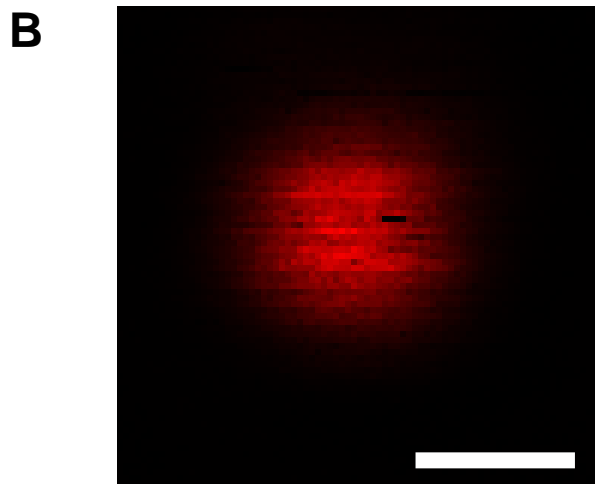
**B**

$$\langle \delta x \rangle_B = 4.1 \text{ nm}$$
$$\langle \delta x \rangle_{SN} = 0.3 \text{ nm}$$

**C****D**



$$\langle \delta x \rangle_B = 0.8 \text{ nm}$$
$$\langle \delta x \rangle_{SN} = 0.3 \text{ nm}$$



$$\langle \delta x \rangle_B = 0.9 \text{ nm}$$
$$\langle \delta x \rangle_{SN} = 0.1 \text{ nm}$$

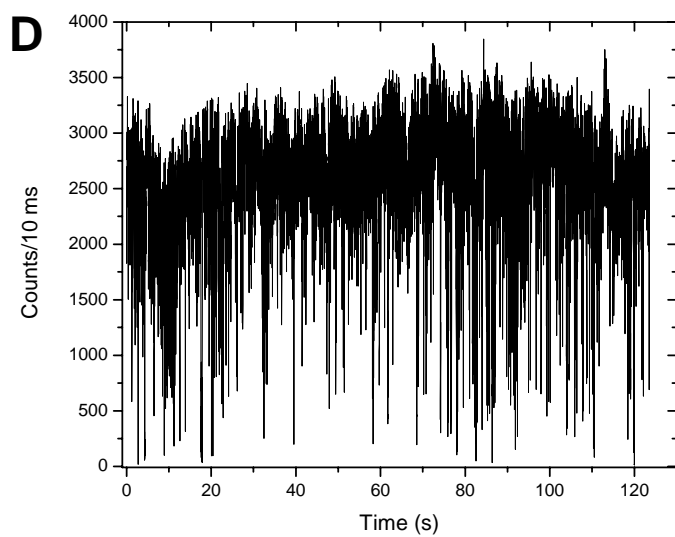
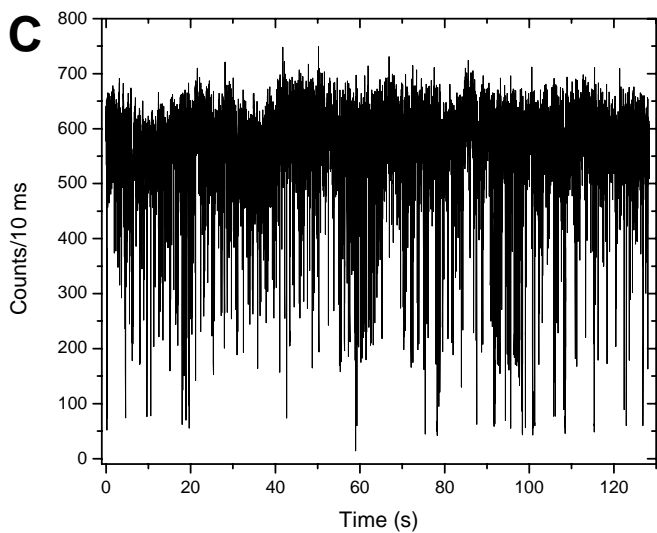


Fig. S2

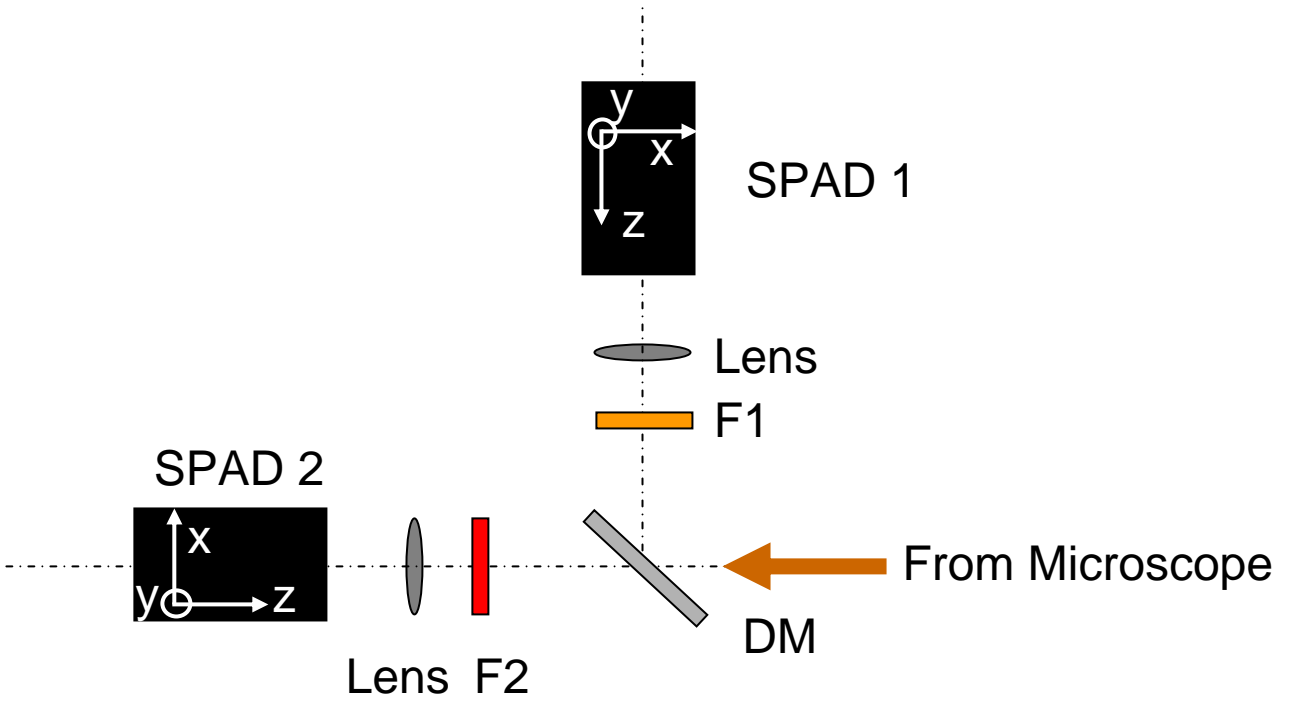


Fig. S3

# SPAD Offset (Fixed Offset)

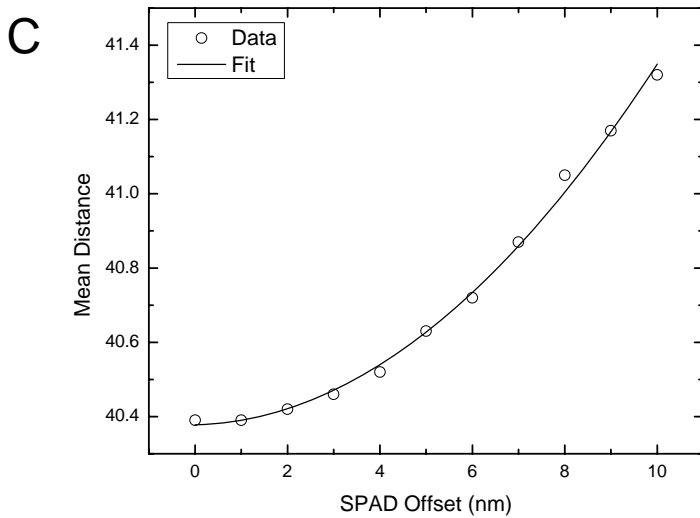
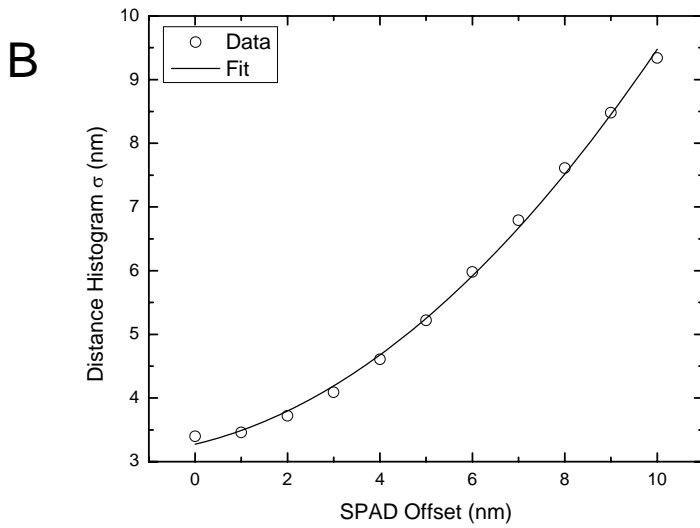
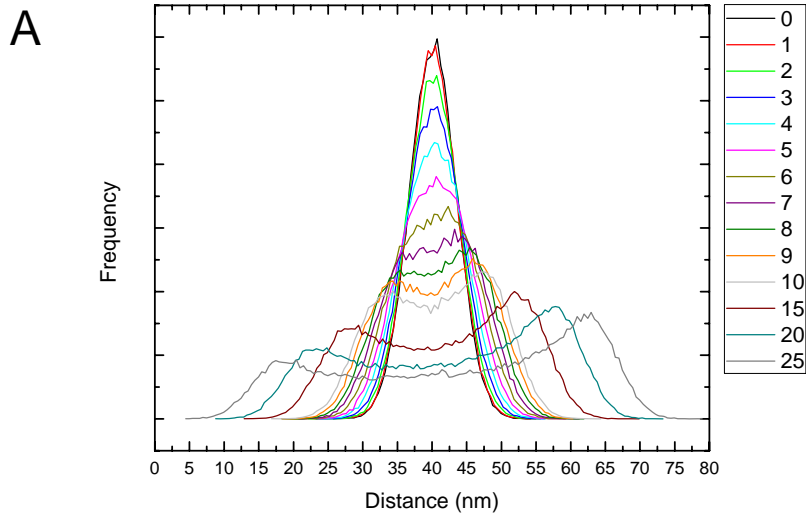


Fig. S4

# SPAD Offset (Variable Offset)

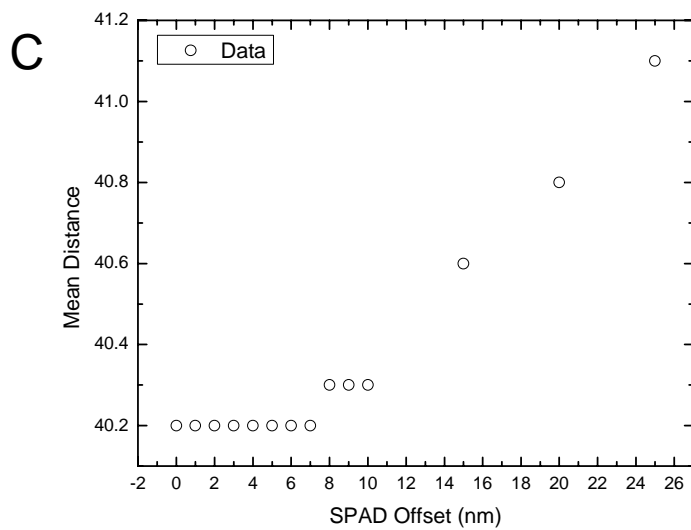
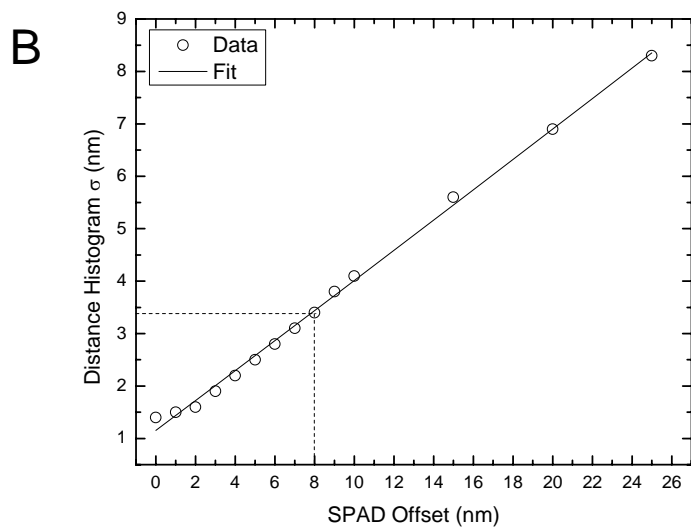
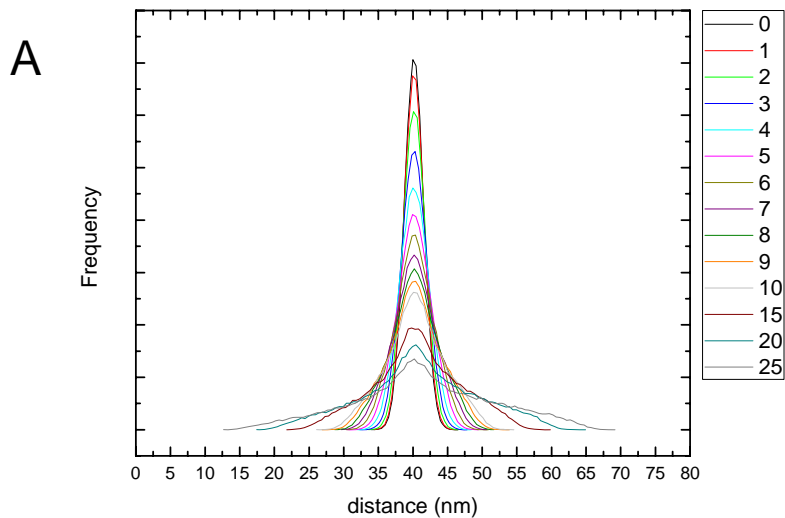


Fig. S5

# Effect of Sigma + Variable Offset

